Influence of Histone Tails and H4 Tail Acetylations on Nucleosome–Nucleosome Interactions

Ying Liu, Chenning Lu,[1] Ye Yang, Yanping Fan, Renliang Yang, Chuan-Fa Liu, Nikolay Korolev and Lars Nordenskiöld*

School of Biological Sciences, Nanyang Technological University, 60 Nanyang Drive, 637551 Singapore

**Corresponding author*: School of Biological Sciences, Nanyang Technological University, 60 Nanyang Drive, 637551 Singapore. Phone: (65) 6316 2812; Fax: (65) 6795 3856; E-mail: LarsNor@ntu.edu.sg

[1]Present address: Department of Cell Biology, Harvard Medical School, Boston 02115

Running title: *Histone tail acetylations and nucleosome interactions*

Keywords: chromatin structure; histone modifications; epigenetic regulation; polyelectrolyte, DNA condensation

Abbreviations: a.a., amino acid; $CoHex^{3+}$, cobalt(III)hexammine, $Co(NH3)_6^{3+}$; DLS, dynamic light scattering; FPLC, Fast protein liquid chromatography; HO, histone octamer; NCP, nucleosome core particle; PA, precipitation assay; SLS, static light scattering; Spd^{3+}, $spermidine^{3+}$, H_3N^+-$(CH_2)_3$-NH_2^+-$(CH_2)_4$-NH_3^+; Spm^{4+}, $spermine^{4+}$, H_3N^+-$(CH_2)_3$-NH_2^+-$(CH_2)_4$-NH_2^+-$(CH_2)_3$-NH_3^+; wt, wild type.

Abstract

Nucleosome -nucleosome interaction plays a fundamental role in chromatin folding and self-association. The cation-induced condensation of nucleosome core particles (NCPs) displays properties similar to those of chromatin fibres, with important contributions from the N-terminal histone tails. We study the self-association induced by addition of cations, Mg^{2+}, Ca^{2+}, cobalt(III)hexammine^{3+}, spermidine^{3+} and spermine^{4+}, for NCPs reconstituted with wild type unmodified histones, with globular tailless histones and for NCPs with the H4 histone tail having lysine (K) acetylations or lysine to glutamine mutations at positions K5, K8, K12 and K16. In addition, the histone construct with the single H4K16 acetylation was investigated. Acetylated histones were prepared by a semi-synthetic native chemical ligation method. The aggregation behavior of NCPs shows a general cation-dependent behaviour similar to that of the self-association of nucleosome arrays. Unlike nucleosome array self-association, NCP aggregation is sensitive to position and nature of the H4 tail modification. The tetra-acetylation in the H4 tail significantly weakens the nucleosome-nucleosome interaction, while the H4 K→Q tetra-mutation displays a more modest effect. The single H4K16 acetylation also weakens the self-association of NCPs, which reflects the specific role of H4K16 in the nucleosome-nucleosome stacking. Tailless NCPs can aggregate in the presence of oligocations, which indicates that attraction also occurs by tail-independent nucleosome-nucleosome stacking and DNA-DNA attraction in the presence of cations. The experimental data were compared with results of coarse-grained computer modelling for NCP solutions with explicit presence of mobile ions.

Introduction

In the eukaryotic cell, nuclear proteins forming regular linear arrays of DNA-histone complexes, the nucleosomes, pack DNA. A central part of the nucleosome is the nucleosome core particle (NCP). The NCP consists of 145-147 bp of DNA wrapped as a 1.70-1.75-turn superhelix around an octamer of the four highly conserved "core" histone proteins, two H2A/H2B dimers and a $(H3/H4)_2$ tetramer.[1-3] Each histone has an unstructured, flexible, N-terminal domain, the "histone tail".[1,4] In the NCP, the tails extend beyond the DNA superhelix and can interact with the DNA of its own NCP, linker DNA and with the other NCPs and proteins present in chromatin. The histone tails are necessary for both secondary and tertiary folding of chromatin[5,6] and significantly contribute to nucleosome-nucleosome interaction.[7] The histone tails are important modulators of the chromatin folding and undoubtedly play significant role in all cellular processes involving DNA, including transcription, replication, repair and recombination.[8,9]

Isolated NCPs display qualitatively similar properties to chromatin fibres in terms of the experimentally observed salt-induced folding and self-association.[10-19] In the NCP, the negative charge of the DNA is only partially neutralized by the histones. Therefore, the NCP carries a significant net negative charge of about −148e, which can be visualized as a central particle (−236e) to which eight flexible and positively charged histone tails (net charge +88e) are attached. Studying the nucleosome-nucleosome interactions in NCP systems is of considerable relevance for understanding chromatin condensation. The NCP-NCP attraction is mediated by the histone tails and was observed in solutions of monovalent salt,[13,16] whereas under similar conditions, free DNA, as well as NCPs and nucleosome arrays lacking the tails, do not show aggregation or folding[6,16] (and references cited in[6]).

A mandatory feature of condensed nucleosome and chromatin structures is the formation of a close NCP-NCP contact between the rather flat surfaces of the globular histone octamer core on both sides of the cylindrical wedge-shaped NCP. Close stacking is observed in NCP crystals[1,2,20,21] (as shown in Fig. 1), in the crystal of the tetranucleosome,[22] and in nucleosome arrays.[23,24] In the condensed structures of NCPs, the stacking is observed in electron microscopy images[15,18,20,25-27] and can also be deduced from X-ray diffraction spectra.[14,15,20,21] The systematic work of Livolant and colleagues analysed the phase behavior of NCP solutions in the presence of cations and gave information on the mechanisms involved in the NCP interactions.[10,12-19,26-28] It was shown that cation-induced NCP aggregation displayed a behavior similar to other polyelectrolyte systems such as DNA.[10] Aggregation of NCPs was found to be dependent on the charge and nature of cations present in solution[10-12,18] and it was concluded that the histone tails mediate NCP-NCP contacts in a salt-dependent manner.[13,16,17,19]

Amino acids in the histone tails are subjected to numerous posttranslational modifications, such as e.g. lysine acetylation, methylation and serine/threonine phosphorylation. Lysine acetylation which results in quenching of the positive charge of the ε-amino group is the most abundant and dynamic modification of the tails. It has been shown that acetylation of histone tails correlate with transcriptionally active regions in chromatin.[29-32] Acetylated chromatin is more easily digested by nucleases,[33,34] and shows higher solubility in monovalent salt (NaCl, KCl) and in the presence of millimolar concentration of Mg^{2+}.[34-36]

Much of the published data on NCP systems was obtained from cell-extracted particles obtained by nuclease treatment of the chromatin[6,11,14,15,18,37] (and references cited therein). These NCPs contain DNA heterogeneous in size and carry an unknown number of post-translational modifications on the histone tails, in particular acetylations.[38,39] Hence, the detailed role and importance of the tails in nucleosome-nucleosome interactions in ordered

precipitated NCP systems and how this interaction is influenced by histone tail acetylations, remains unclear.

Only recently, large quantities of precisely positioned and fully saturated NCPs and nucleosome arrays have become available. These well-defined chromatin models can be obtained using recombinant histones and DNA with a sequence that has high nucleosome affinity. Using these objects, determination of the contributions of individual tails and specific alterations within them (acetylation, phosphorylation, mutations etc) to the self-association of chromatin and NCPs is now possible, and a growing number of works performed on recombinant chromatin and NCPs prepared by recombinant methods are emerging.[17,19,23,40-48] There is, however, only a limited amount of data available for systems with modifications of the individual histones, such as mutants lacking tails, containing only the globular part of the histone molecule,[17] or with selected tail lysines replaced by glutamine (K→Q mutation), mimicking acetylation.[23,40-45] Published results indicate that lysine acetylation or absence of tails stabilize NCPs or arrays in the solution state over self-association and promote the unfolding of compact nucleosome arrays.[17,40-42,47,49] The H3 and H4 tails[17,41,50,51] and specifically H4K16,[40,44,47] have been found critical for intramolecular folding of individual nucleosome arrays. Noteworthy, one of the H4 K16-R23 regions (of the two H4 tails) is clearly involved in NCP-NCP stacking since it is located between the two NCPs in practically all reported NCP crystal structures. Figure 1 uses the first reported atomic resolution NCP structure 1AOI[1] to illustrate the stacking and the role of the H4 tail K16-R23 domain in mediating the nucleosome-nucleosome interaction.

In the present work we investigate nucleosome-nucleosome interactions induced by addition of the cations, Mg^{2+}, Ca^{2+}, cobalt(III) hexammine ($Co(NH_3)_6^{3+}$, $CoHex^{3+}$) and the natural polyamines spermidine^{3+} (Spd^{3+}) and spermine^{4+} (Spm^{4+}), by studying NCPs reconstituted with various forms of histones. Wild-type (wt) and mutant NCPs were

reconstituted from recombinant *Xenopus laevis* histones with the 147 bp palindromic human α-satellite DNA fragment[1,2] or with the 145 bp fragment of the Widom '601'[52] nucleosome positioning sequence. In addition, NCPs containing the H4 histone with lysines acetylated at the H4K16 position (H4-K16Ac), with tetra-acetylated H4 histone (at the positions K5, K8, K12, and K16, denoted quadAc-NCP) were studied. The acetylated forms of the H4 histone were synthesized using a novel method combining solid state peptide synthesis and native chemical ligation.[47] To compare the effect of acetylations and lysine to glutamine mutations, NCPs containing mutations in the H4 amino-terminal (K5, K8, K12, and K16 positions, quadQ-NCP) were studied. To the best of our knowledge, this is the first time that the cation-dependent aggregation has been studied for well-defined recombinant mononucleosomes. We compare the results for the wild type unmodified histones, with observations for NCPs having well-defined acetylations and K→Q mutations in the H4 tail. The data give information on the importance of these modifications for the nucleosome-nucleosome interactions. Additionally, NCPs containing all four histones in the N-terminal truncated form (tailless globular NCP, denoted g-NCP) were studied.

The experimental results were compared with data from computer modeling, using our recently-developed coarse-grained model of the NCP[47,53] in solutions with explicit consideration of the mobile ions. This model is based on a continuum description of the solvent and focuses on effects caused by the electrostatic interactions such as ionic screening, ion-ion correlations and competition, tail bridging and ion valence.[46] The modeling results underline the major role of unspecific long-range electrostatics and histone tail mediated interactions in the NCP system.

Results and Discussion

Electrostatic mechanism of NCP aggregation

Figure 2 displays the results of studying the wt-NCP aggregation upon addition of Mg^{2+}, Ca^{2+}, Spd^{3+}, $CoHex^{3+}$ and Spm^{4+} ions monitored by precipitation assay (PA) (Fig. 2a) and by static light scattering (SLS) (Fig. 2b). Additional titrations curves are shown in the Supplementary Material Figure S1 and S2. Table 1 summarizes the EC_{50} values obtained in these titrations. EC_{50} is the cation concentration at 50% of the maximal aggregation (in PA) and the concentration at 50% intensity in the SLS curve, both obtained by sigmoidal fitting, unless otherwise noted. For the wt-NCP data, the maximal precipitation is larger than 95% and EC_{50} is then practically the same as $C_{50\%}$, which reflects the cation concentration at a 50% reduction of the NCP concentration in the supernatant in the PA measurements. The two types of measurements were conducted at different NCP concentrations. For the PA titration, the NCP concentration, C_{NCP}, was 0.55 μM (equal to 162 μM of DNA phosphate concentration, C_p). In the SLS titration, the NCP concentration was either 0.068 μM (C_p=20 μM) or 0.034 μM (C_p=10 μM). Data were obtained for two different salt conditions: 1) In 10 mM Tris·HCl buffer, pH 7.5 (Table 1, Supplementary Material, Fig. S1 and S2; at the given pH concentration of the $Tris^+$ the cations in solution is about 8 mM). 2) In solution of 10 mM Tris·HCl, pH 7.5 plus 10 mM KCl (Table 1 and Fig. 2). For all systems, we used NCPs reconstituted with the human 147 bp α-satellite DNA. Additionally, experiments in 10 mM Tris·HCl buffer were also carried out for, for wt-NCPs reconstituted with a 145 bp DNA Widom "601" sequence (Table 1, row 1 and 4, Supplementary Material, Fig. S1 B and C); see below and Materials and Methods.

As we can clearly see in Figure 2, the potency of the cations to induce wt-NCP aggregation follows the order: $Spm^{4+} > CoHex^{3+} > Spd^{3+} >> Ca^{2+} \geq Mg^{2+}$. This result underlines a typical polyelectrolyte behavior with a critical importance of the charge of the added cation as the major factor determining the critical concentration needed to induce aggregation. An increase of the cation charge from +2 to +4 shifts the EC_{50} value by three

orders of magnitude, from the millimolar range for Mg^{2+} and Ca^{2+} to micromolar for Spm^{4+} (Table 1, Fig. 2, Supplementary Material, Fig. S1 and S2). A similar order and range of EC_{50} values were observed for NCPs reconstituted with modified H4 histones (see below). This is a clear indication of the polyelectrolyte nature of the NCP, which has its origin in the high negative charge of the DNA that is only partially neutralized by the positive charge of the histone octamer. It should also be noted that a qualitatively, comparable cation dependent self-association behavior has also been observed for nucleosome arrays.[46,47,54] The precipitation and light scattering titration curves also show an apparent similarity to data obtained for DNA.[55,56] However, it is known[57,58] that divalent cations are unable to condense DNA in water solution, while in the case of NCPs, Mg^{2+} and Ca^{2+} induce attraction, leading to aggregation and almost complete precipitation. Similar NCP precipitation induced by cations Mg^{2+} [11,18] and Ca^{2+} [11] was described earlier by Livolant and co-workers. However, the difference in NCP samples, NCP concentration and other conditions of the experiments excludes a quantitative comparison with previous studies. It may be emphasized that we use recombinant histones and well-defined DNA, compared to NCPs obtained from calf thymus chromatin by micrococcal nuclease digestion,[11,18] which produce a NCPs with a distribution of the DNA length and histones that are likely have a considerable extent of undefined post-translational modifications in the tails.[38]

In the presence of cations of charge exceeding +2, (Spm^{4+}, $CoHex^{3+}$ and Spd^{3+}), the addition of 10 mM K^+ shifted the EC_{50} values towards higher cation concentration as observed in both PA and SLS titrations (Table 1, Fig. 3a, b and d, stars, Fig. S3 B). For Mg^{2+} and Ca^{2+} this change of EC_{50} is similar but less pronounced. This shift is expected, based on the strong salt dependence of the polyelectrolyte aggregation and had previously been characterized in detail for DNA.[55]

Removal of two base pairs from the DNA (147 and 145 bp) slightly reduces the magnitude of the negative charge on the NCP (by −4e) and this is reflected by a decrease of the EC_{50} values. The difference between the EC_{50} values for the 147 and 145 bp DNA NCPs generally becomes smaller with increase of cation charge (Table 1; the exception is the light scattering data for $CoHex^{3+}$). However, the observed difference in the EC_{50} values for the NCPs with 147 and 145 bp DNA (e.g. Spd^{3+}) is too large to be explained solely by an electrostatic effect caused by the rather small reduction of the DNA negative charge. We noted that reconstitution with 145 bp DNA (using the Widom '601' nucleosome positioning sequence) produced NCP solutions that were more homogeneous and temperature resistant as well as being more stable during storage than the NCPs reconstituted with 147 bp DNA (human α-satellite sequence). Additionally, NCPs with 145 bp DNA gave a lower content of off-centered DNA-positioned nucleosomes which could be more easily and completely repositioned compared to 147 bp DNA NCPs. Therefore, it is likely that (in addition to the difference in the net charge) variations in homogeneity and in structures between 145 bp and 147 bp NCPs influence the EC_{50} values. A recent small angle X-ray scattering study[59] reported that NCPs reconstituted with the Widom '601' sequence retains the shape observed in the crystal while NCPs with the human α-satellite DNA show SAXS profiles which can only be explained by assuming a change in the NCP structure consistent with partial unwinding of the DNA from the histone octamer. Such an effect is likely to change the quantitative, but not qualitative, aggregation behavior of NCPs reconstituted with different nucleosome positioning sequences.

Increase of the NCP concentration requires larger amount of cation to neutralize the negative charge of the NCP and, as expected, generally gave higher EC_{50} values for the PA results as compared to the SLS data (Table 1). Exceptions are the SLS results for Mg^{2+} and Ca^{2+} (C_p = 10 μM or 20 μM) that gave EC_{50} values higher than those obtained in the PA

experiment (C_p = 162 μM). It is worth noting that a similar odd shift of EC_{50} was recorded for DNA condensation by $CoHex^{3+}$.[55]

If the titration experiments are continued to higher cation concentrations, re-solubilization of the NCPs to an isotropic solution is observed.[10,11,18] Since this effect is rather irrelevant to the *in vivo* conditions, in the present work, we intentionally did not investigate the range of such high concentrations where this phenomenon is observed.

Complete tail deletion or H4 tail acetylations, dramatically impedes NCP aggregation

Figure 3 compares aggregation of the wt-NCP and tailless globular NCP (g-NCP) systems determined in titration experiments by the PA (Fig. 3a,b and Fig. S3 B) and SLS (Fig. 3c,d) methods. Tables 2 and 3 report data determined from these titrations. In addition to the data for wt-NCPs and g-NCPs, Tables 2 and 3 contain information on aggregation properties of the AcK16-NCP, quadAc-NCP and quadQ-NCP (see Fig. 4 that compare PA results for NCPs with the various histone variants, and Supplementary Material Fig. S3 A for PA titration of quadQ-NCP with all five cations). Complete precipitation was not achieved by addition of Mg^{2+} or Ca^{2+} in the systems of tetra-modified and g-NCPs. Therefore, $C_{50\%}$, which reflects the cation concentration at 50% precipitation of the NCPs, was used to quantify the efficiency of the cations in inducing the aggregation in these systems. For the situations when 50% precipitation was never achieved, the concentration at the maximal precipitation is quoted in Table 2.

Removal of the histone tails decreases the tendency of the g-NCP to aggregate and leads to higher values of $C_{50\%}$ (PA) and EC_{50} (SLS) (Fig. 3, Tables 2 and 3). Histones refolded to globular HO were designed to match the histone amino acid sequence after trypsin digestion so that a total of 56 positive charges were removed compared to the net charge of the wt-HO. The net charge of the 'globular' histone octamer is +92e (the globular part of the HO plus the

remaining short stretches of the truncated tails). Addition of the divalent cations Mg^{2+} and Ca^{2+} leads to incomplete precipitation of g-NCP (50-60%; Fig. 3a, Table 2) and to the formation of aggregates as observed by light scattering, although with lower scattering intensity as compared to wt-NCP (Fig. 3c,d, Table 3). In 10 mM Tris·HCl buffer, aggregation induced by Mg^{2+} showed the most significant difference between wt-NCP and g-NCP with a 9-fold increase in the EC_{50} value for g-NCP in the SLS titration (Table 3) and a 15-fold increase in the $C_{50\%}$ obtained by the PA titration (Table 2). The tail bridging mechanism that contributes to the nucleosome-nucleosome interaction in wt-NCP is lacking for g-NCPs. It is known that addition of divalent ions cannot precipitate free DNA.[57,58] Literature data[57,58] for DNA were usually obtained for high molecular weight DNA. For comparison with our NCP systems, we therefore carried out a number of control SLS and PA Mg^{2+}-titrations with solutions of 147 bp DNA and found no light scattering intensity increase in the SLS experiments and limited precipitation in the PA (below 25% at high Mg^{2+} and Ca^{2+} concentrations, Table 2, Supplementary Material Fig. S3 C). In the g-NCP, the charge density of DNA wrapped around the HO core, is reduced compared to naked DNA. DNA has a higher negative charge compared to the tailless NCP, where the net positive charge (+92e) of the octamer (the globular domain plus the remaining tail fragments) effectively reduce a substantial fraction of the net charge of the 147 bp DNA (–294e). Based on polyelectrolyte behavior, the tailless g-NCP system is not expected to display any significant attraction in the presence of divalent ions that would lead to aggregation. Remarkably, however, the addition of the divalent cations Mg^{2+} and Ca^{2+} (Fig. 3a Table 2) still leads to 50-60% precipitation of the g-NCP and to the formation of aggregates as observed by light scattering, although with lower scattering intensity as compared to wt-NCP (Fig. 3c,d, Table 3), see further comment below. It therefore appears that NCP-NCP stacking in itself may favorably contribute to NCP

attraction in the presence of divalent cations (perhaps with some small contribution from remaining stretches of the histone tails).

Precipitation of g-NCPs induced by the trivalent $CoHex^{3+}$ showed a less dramatic difference in the $C_{50\%}$ value compared to wt-NCP; about two-fold increase (Table 2; see values determined in 10 mM Tris buffer). However, an interesting observation surfaces while comparing the EC_{50} value of g-NCP with that of control DNA. In spite of the lower charge density of the g-NCP (compared to control 147 bp DNA), the $C_{50\%}$ value is considerably lower for the g-NCP (67 μM compared to 94 μM for 147 bp DNA; Table 2). The observations in the presence of divalent and trivalent ions therefore indicate a contribution to attraction leading to the condensation of NCPs, originating from nucleosome-nucleosome interactions (even without the mediating effects of the histone tails), in addition to attractive DNA-DNA interactions due to ion correlation in the presence of multivalent ions.

Acetylation of the single H4K16 residue induces a pronounced shift in the aggregation behaviour of the wt-NCPs in the presence of Mg^{2+}. The $C_{50\%}$ value for the K16Ac-NCP is larger than the corresponding values of the wt-NCP (2.3 mM compared to 1.4 mM; see Table 2). Lysine acetylation at the four positions (quadAc-NCP) makes a significant influence on the NCP aggregation. In the case of Mg^{2+}, the value $C_{50\%}$ increases more than 4 times relative to the wt-NCP (Table 2), while the quadQ-NCP system moderately changes the $C_{50\%}$ value (see Table 2, first column in Tris buffer; $C_{50\%}$ is 3.1 mM for quadQ-NCP compared to 5.9 mM for quadAc-NCP and 1.4 mM for the wt-NCP). When aggregation of the NCPs is induced by the more efficient cation, $CoHex^{3+}$, the differences in precipitation behavior between various NCPs become less significant. The $C_{50\%}$ values increase from 37.2 μM for the wt-NCP to 67 μM for the g-NCP. Still, the effect of the single H4-K16 acetylation as well as the difference between tetra-acetylated and tetra-mutated H4 histones is discernible (Table 2, $CoHex^{3+}$ in Tris buffer). Figure 4 shows the effects of the H4 mutations and acetylations in

comparison with the data for wt-NCP, illustrated with the PA data for both divalent (Mg^{2+}) and trivalent ($CoHex^{3+}$) cations. This data indicates that NCP self-association is dependent on the type of the H4 histone modification since there are significant differences between quadAc-NCP and quadQ-NCP.

The trivalent cation, $CoHex^{3+}$, produces more densely packed NCP aggregates than the divalent Mg^{2+} and Ca^{2+}, as reflected by the high intensity of light scattering at the end of SLS titration (Table 3, Fig. 3c,d). This effect is more apparent for the wt-NCP and quadQ-NCP (see Table 3). (The similar light scattering intensities for divalent and trivalent ions in the case of the g-NCP is likely caused by a five-time difference in NCP concentrations applied in $CoHex^{3+}$ and Mg^{2+}/Ca^{2+} titrations.) The maximal signal intensity for divalent cations is around 300-500 kcp for wt-NCP and 180 kcp for the quadQ-NCP. For all cations there is a substantial difference in signal intensity observed between wt-NCP and g-NCP. A high signal is observed for wt-NCP while the intensity is considerably lower for g-NCP (comparing solutions with equal NCP concentrations, see e.g. Table 3, rows two and four). Dynamic light scattering analysis indicated that particles of similar or larger size were formed by g-NCPs (data not shown). The intensity of the light scattering signal is defined by the particle size and the difference in the refraction indices between the particle and the solvent. This observation therefore indicates that the globular NCPs forms loose swollen aggregates (containing more water) compared to the particles formed by the wt-NCPs. In addition to the higher values of EC_{50} for the g-NCP comparing to the wt-NCP, titration curves of the globular NCP display a broader range of transition (Fig. 3c,d). It is also observed that the quadQ-NCP system display particle formation with lower scattering intensity as compared to wt-NCP, while the aggregate sizes are comparable (data not shown).

Comparison of NCP aggregation with nucleosome array folding and self-association

It is interesting to compare the experimental precipitation assay data obtained for the NCP in the present study with the results on condensation of nucleosome arrays reported in our recent paper.[47] In the cited work, fully saturated nucleosome arrays consisting of 12 nucleosomes with a nucleosome repeat length 177 bp were prepared using either H4 wild type, H4K16 acetylated, H4K16Q mutated, or H4 K5+K8+K12+K16 acetylated and K→Q mutated histones (the other 3 core histones were full-length unmodified recombinant *Xenopus laevis* histones). During condensation of the nucleosome arrays, it is possible to register two processes: internal folding of the array into 30-nm fiber and intermolecular aggregation (self-association). The former process is monitored by analytical ultracentrifugation; the latter one is studied by precipitation assay designed similarly to the PA applied for the nucleosome solution. Since both set of results (for the NCP and for the arrays) were obtained using the same histone preparations, similar DNA concentration and the same experimental protocol, the differences between the data can be attributed to possible alternative mechanisms of self-association as well as to differences in structures of the aggregated phases of the NCP and array.

The major conclusions from studying the array self-association using PA method were:[47] i) Both acetylations and K→Q mutations in the H4 histone tail produced an identical increase of the EC_{50} values. ii) Single H4K16 acetylation or K→Q mutation did not make a significant influence on the array self-association, with identical modest effects compared to the wild type array. iii) A non-specific electrostatic mechanism governs the array self-association (namely, EC_{50} is dependent on the total number of positive charges quenched in the histone tails with no special sensitivity to the position or nature of the charge alteration). The sensitivity to the nature of the Lys alteration (acetylation or K→Q mutation) was observed only for the process of internal folding of the array.[47] Interestingly, for the mononucleosomes, precipitation behavior showed some features which make NCP aggregation look somewhat

similar to the array folding. Noticeable differences were observed between the EC_{50} (or $C_{50\%}$) values of the quadAc-NCP and quadQ-NCP and between wt-NCP and K16Ac-NCP for Mg^{2+}-induced precipitation (see Table 2, first column in Tris buffer and Fig 4a). The data for $CoHex^{3+}$ (Table 2, Fig 4b) were closer but a difference between quadAc-NCP and quadQ-NCP was still observed. This variation in array and NCP aggregation behavior indicates that NCP aggregation is more sensitive to the structural aspects of the NCP-NCP interaction while array self-association is more unspecific. In this respect, aggregation of the NCPs is somewhat similar to the intramolecular folding of the array, which showed a strong sensitivity to H4-K16 acetylation but not to H4K16Q mutation (both for single H4K16 site and tetra-acetylated/mutated variants of the H4 histone).[47] This implies that aggregated NCP involves nucleosome-nucleosome stacking with structural elements similar to these observed in internal folding of the array. This inter-nucleosome interaction includes binding of the H4 histone K16-R23 domain of one NCP to the so-called "H2A acidic patch" on the surface of the other NCP (see Fig. 1),[1] combined with the recently discovered interaction of the H4-K16 ε-amino group (of the same K16-R23 domain) with the main-chain carbonyl groups of the R96-L99 amino acids in the H2B histone.[47]

Computer modeling confirms the electrostatic mechanism of NCP interactions

In order to gain an understanding of the importance of the general unspecific electrostatic interactions to the attraction and subsequent aggregation of the NCP solution, caused by the addition of multivalent ions, we performed Langevin molecular dynamics computer simulations of a system of ten NCPs in a dielectric continuum model with explicit presence of mobile ions representing the various cations. The NCPs are modeled with our previously described coarse-grained electrostatic model consisting of a central sphere representing the HO with DNA in the form of connected beads wrapped around it.[46] Attached to the HO are flexible charged "histone tails" in the form of connected charged beads. This model is

illustrated in the Supplementary Material (Fig. S4). Figure 5a visualizes different effects of the addition of cations of varying charge to the simulation systems. Representative snapshots illustrate the NCP-NCP aggregation for wt-NCPs with complete and fully charged tails. Parameters calculated from the simulations are presented in Tables S1-S3 of the Supplementary Material**.** The results illustrate a qualitative behavior similar to the experimental observations, with an inability of elevated concentrations of monovalent cations to induce attraction between NCPs and with the tetravalent Spm^{4+} being the most potent ion in eliciting the aggregated state. In Fig. 5b, the attractive nature of the NCP-NCP interactions in the presence of divalent (blue curve) and trivalent (red curve) cations is emphasized by the core-core radial distribution functions (RDF). Peaks around 10-12 nm are indicative of close interactions, the nature of which is sketched by the inset illustrations of representative contacts. The importance of the histone tails in mediating this attraction is illustrated in Fig. 5c that shows the external tail-core RDF for systems with K^+, Mg^{2+}, Spd^{3+}, $CoHex^{3+}$ and Spm^{4+} ions. This RDF gives information on the presence of tail bridging. In solution with monovalent cations, NCPs always repel each other and there are no contacts between cores and tails of different NCP. It is evident that such contacts are frequent for the systems showing attraction and are strongly pronounced in the presence of the most potent condensing agents, Spm^{4+} and $CoHex^{3+}$.

Comparing the tailless and wt-NCPs, we observe that the globular NCPs show a diminished tendency to aggregate. In the presence of $CoHex^{3+}$, the g-NCPs occasionally form short-lived aggregates of 2-3 particles. Under similar conditions, all ten wt-NCPs form a single dense aggregate (see corresponding snapshots in Fig. 5a). Qualitatively this is in agreement with the experimental observation that larger concentrations of the trivalent cations are needed to invoke attraction for tailless NCPs. Figure 5b also compares core-core RDFs of the wt-NCP and g-NCP in the Mg^{2+}- and $CoHex^{3+}$-containing systems. In the system

of g-NCPs with Mg^{2+}, the NCP-NCP interaction is always repulsive. At a comparable Mg^{2+} concentration, wt-NCP shows considerable aggregation (solid blue curve in Fig. 5b). The attraction between g-NCPs in the presence of $CoHex^{3+}$ is clear from the peak in the RDF, but it is weak. The observation of weak (for $CoHex^{3+}$) or absence of (for Mg^{2+}) NCP-NCP interaction in the simulations of these tailless NCPs, is somewhat different from the experimental results showing some (for Mg^{2+}) or complete (for $CoHex^{3+}$) aggregation in solutions of g-NCPs (see discussion in the next section).

Figure 6 presents the data obtained for systems of wt-NCPs, NCPs with each H4 tail having four charges quenched (denoted quad-NCP, mimicking quadAc-NCP/quadQ-NCP) and g-NCPs. The amount of multivalent cation is progressively increased in a series of simulations, where monovalent ions are replaced by the oligocation, qualitatively mimicking a "titration" experiment. The core-core contact number gives an estimation of the number of NCPs which are in a close contact with each other. It is observed that the highly potent condensing-agent, $CoHex^{3+}$, is capable of complete condensation of wt-NCPs or quad-NCPs, while smaller aggregates are formed in the case of globular NCPs. In the presence of Mg^{2+}, the wt- and the quad-NCP systems show different degree of compaction in qualitative agreement with experiments. In the presence of $CoHex^{3+}$, the results for wt- and quad-NCP are very similar; in qualitative agreement with experiments. It is of interest to compare the results of Fig 6a and 6b (which show respectively core-core contacts and tail bridging during the "titration"). There is a clear correlation in the increased attraction as reflected by the increased value of the core-core contact number, with the increase in tail bridging. The modeling results therefore gives information on the importance of the tail bridging mechanism to aggregation of NCPs, induced by increasing oligocation concentration.

Comparison of experimental and modeling results

Results of the present MD simulation on the NCP-NCP interaction are in agreement with our earlier data, using a simpler model (the globular part of the NCP modeled as one single sphere), studying the influence of the ionic conditions (K^+ and Mg^{2+} concentration)[60] and tail modifications.[53] The good agreement between the modelling results obtained using two different NCP models, confirms that long-range electrostatic interactions dominate the cation induced NCP aggregation process.

Quantitative comparison of experimental and simulation results is not possible due to the considerable differences between conditions of the MD simulation and in the test tube. In the simulations, the NCP concentration, C_p, (the DNA phosphate concentration) is 77 mM and the constant small amount of added monovalent salt about 5 mM, which corresponds to a ratio $C_{salt}/C_p = 0.06$. In the experiments, the NCP phosphate concentration is much lower (C_p = 0.162 mM and 0.010-0.050 mM for the PA and SLS methods respectively). Additionally, there is a huge excess of added salt relative to the net NCP concentration. For solutions with 10 mM KCl, the ratio C_{salt}/C_p is approximately equal to 60 for the PA and up to 1000 for the SLS experiments (at C_p =10 μM). Even in the absence of KCl, the ionic strength due to the Tris buffer is large compared to the NCP concentration (approximately 8 mM $Tris^+$ cations in the 10 mM Tris·HCl buffer at pH 7.5). It is not possible to perform simulations with the large box size and large number of particles that would correspond to these conditions.

Consequently, it is not possible to compare the absolute cation concentrations that lead to pronounced attraction in the simulations (Fig. 5), with the $C_{50\%}$ concentrations characterizing the precipitated state in the experiments. E.g., from Table 2 we find that for wt-NCP, the charge ratio, $CR=C_{cation}\cdot Z/C_{negative}$, at $C_{50\%}$ is 60.5 for Mg^{2+} and 2.16 for $CoHex^{3+}$. Here the charge ratio is the concentration of the oligocation charge, $C_{cation}\cdot Z$ (Z is the oligocation charge), relative to the net (i.e. after neutralization by the histones) NCP charge concentration, $C_{negative}$. In the simulations, the values of CR are 1.07 for both Mg^{2+} and

$CoHex^{3+}$ under conditions of maximal attraction. (CR values relevant to the simulation conditions are provided in the Supplementary Material, Tables S1-S3).

Therefore, the results of the simulations should be analyzed on their own and only the general qualitative trends can be qualitatively compared with the experimental results. It is clear that the simulations do reproduce the qualitative trends observed in experiments. Importantly, the simulations exhibit typical polyelectrolyte behavior as manifested by the inability of monovalent cations to induce aggregation and the considerably stronger attractions between NCPs in the presence of the trivalent $CoHex^{3+}$ (as compared to divalent ions like Mg^{2+}). Additionally, the effects on the core-core contact numbers (see Fig. 6a, comparing wt-NCP and quadQ-NCP) illustrate a modest effect on NCP aggregation due to the H4 tail charge quenching of the four lysines. This is the expected behaviour for an electrostatically controlled mechanism as the quenching of eight out of 88 positive charges among all tails, would only slightly change the quantitative behavior. This is also observed in the experiments, since this histone modification has limited effect on the $C_{50\%}$ values (Table 2). The more pronounced effect with quadAc-NCP, observed mainly for divalent Mg^{2+}, therefore indicates the presence of a more specific mechanism, probably originating from H4K16, in the interaction between stacked nucleosomes.[47]

The complete absence of attraction in the presence of divalent ions, as shown in the simulation results for g-NCP, is in fact the expected behavior for a purely electrostatic coarse-grained model as the present one. As mentioned above, the experimental observation of attraction for g-NCP in the presence of divalent ions is contrary to expectations based on polyelectrolyte theory, given the absence of tails that excludes the contribution from the attractive tail bridging to the interaction between NCPs. These observations are interesting and the comparison between the modeling and experimental results therefore indicate that short ranged specific nucleosome-nucleosome interactions, even in the absence of histone

tails, contribute to the aggregation of NCPs. The present coarse-grained model lacks the detailed description of the geometry and charge distribution in the NCP and as such cannot account for a number of specific effects such as charge-charge, hydrogen bonding and hydrophobic interactions. Therefore, the discrepancy between experimental and modeling results in fact gives important information about the presence and scale of the interactions that are not included in the present simulation approach, which aids in further development and design of the model.

Conclusions

Using well-defined nucleosome core particles prepared by recombinant methods, we found that the attraction between the NCPs, induced by the addition of varying oligocations, follows a similar polyelectrolyte behavior as DNA condensation and that it is also similar to the self-association of well-defined nucleosome arrays. From literature, it is known[15,18,20,26,27] that NCPs form columnar stacks of particles and it is believed that the nucleosome-nucleosome interaction leading to this stacking is mediated by the histone tails. By studying NCPs with specific acetylations in the H4 tail, the importance of the H4 lysines, to the stacking mechanism is highlighted. The importance of the histone H4 lysine K16 to the nucleosome-nucleosome interaction that we observed is similar to its role in chromatin folding, as observed in the studies of nucleosomal arrays.[40,44,47] Even in the complete absence of all the tails, nucleosome-nucleosome attraction is pronounced and stronger than expectations based on the expected polyelectrolyte electrostatics and leads to partial aggregation in the presence of divalent Mg^{2+}. Whether this means that nucleosome-nucleosome stacking resulting in a columnar phase, is present in the absence of the histone tails remains to be investigated by X-ray scattering methods.

Materials and Methods

NCP reconstitution

Palindromic human α-satellite DNA (147 bp)[2] was prepared in several steps using the plasmid pUC19 vector with the p32-α8s-147 construct that contained 32 repeats of 84 bp DNA sequences, each including 72+3 bp (72 bp + 3 nucleotide overhang) half-site of the target 147 bp. The preparation was carried out according to the protocols[61-63] and included plasmid amplification (in *E.coli* HB101 strain) and extraction; *EcoRV* digestion (to generate 84 bp fragments); 84 bp fragment isolation, dephosphorylation and *HinfI* digestion (to produce 72+3 bp DNA half-site); ion exchange (Mono Q 5/50 GL column) purification of the 72+3 bp DNA half-site; ligation of the half-site fragments by the T4 DNA ligase; and ion exchange purification of the 147 bp DNA. Preparation of the 145 bp DNA included amplification of the pUC57 plasmid containing eight copies of the 145 bp Widom '601' sequence[52] (EZBiolab, Carmel, IN, USA) followed by *EcoRV* digestion and DNA purification as described.[3,61-63]

Histone expression, purification and histone octamer (HO) refolding was performed as described in our previous work.[46,47] Full length *Xenopus laevis* histones H2A, H2B, H3 and H4 were individually expressed in *E.coli* (BL21 (DE3) pLys S). Each of the histones was purified by gel filtration on Hi prep 26/60 Sephacryl S-200 column (ÄKTA FPLC, Uppsala, Sweden).[61] Further purification was carried out on Resource S cation exchange column (ÄKTA FPLC). Histone H4 with K→Q mutations at positions 5, 8, 12, and 16 (prepared by site-directed mutagenesis) as well as tailless histones[50] were prepared from mutated and truncated constructs, respectively. The tailless histones are truncated as follows: wt-H2A(1-129) → g-H2A(13-118); wt-H2B(1-122) → g-H2B(22-122); wt-H3(1-135) → g-H3(27-135) and wt–H4(1-102) → g-H4(20-122), thus including H2A C-terminal deletion as well. The expression and purification of the mutated and globular histones followed that of full length histones. HO refolding required more cautious optimization of the ratio of the each histone

components. A number of experiments have also been carried using NCPs reconstituted with acetylated histone H4 at the position Lys 16 (AcK16-NCP) and at the quadruple sites Lys 5, 8, 12 and 16 (quadAc-NCP). The acetylated H4 histones were prepared using a novel approach combining solid state peptide synthesis and native chemical ligation as described.[47]

Histone octamer with wt, acetylated or tailless H4 histone were refolded using a 1:1:1.2:1.2 molar ratio for H2A, H2B, H3 and H4 respectively.[61] Histone octamer with mutated H4 histone were refolded using a 1:1:1.5:1.5 molar ratio instead. The octamer was purified by gel filtration on the Sephacryl S-200 high resolution gel filtration column (GE Health Care).[61] The quality of reconstituted octamers was checked by resolving individual histones in 18% SDS PAGE (Fig. 7a).

Nucleosome core particles were produced through dialyzing purified histone octamer and 147 bp or 145 bp DNA fragments at appropriate ratio over an exponential gradient, with decreasing KCl concentration. Five types of NCPs, namely wild-type (wt-NCP), NCP with H4 histone containing the single H4K16 acetylation (AcK16-NCP), as well as quadruple acetylated (quadAc-NCP) or K→Q mutated (quadQ-NCP) histone H4 at Lys 5, 8, 12, 16 and NCPs with all four histones lacking N-termini (globular NCP, g-NCP), were reconstituted following protocols described in[62,63] with appropriate modifications. The DNA:HO ratio was optimized by testing HO: DNA molar ratios 0.8, 0.85, 0.9 and 1.0 in small scale preparations. A volume of 200 µl containing 6 µM (0.544 mg/ml) 147 bp DNA and the respective amount of HO was used. The optimal ratio was found to be around 0.9:1 and varies somewhat between batches (see Supplementary Material, Fig. S5, for illustration with g-NCP). The presence of NCPs due to off-centered DNA (Fig. 7b) can be removed by heat shifting that increases the population of well-centered DNA on the HO. During reconstitution, the solution was dialyzed from the EDTA-free high-salt buffer (1.3 M KCl, 20 mM Tris-HCl, pH 7.5, and 1 mM DTT) towards the low-salt buffer containing 20 mM Tris-HCl (pH 7.5) and 1 mM

DTT. The process was automated using a peristaltic pump and lasted for 36 hr. Precipitates were removed by triple centrifugation (9,000g×5 min.) at 4˚C. The quality of the NCPs was examined by 5% PAGE (Fig. 7b). To generate large quantities of the NCP, the reconstitution was scaled up in a volume from 1 to 3 mL.

Static light scattering (SLS)

Static light scattering (SLS) experiments were conducted using a Brookhaven 90plus particle size analyzer (Long Island, NY) at 25˚C as described earlier.[64] Three concentrations of NCP were used (0.034, 0.068 or 0.17 μM NCP; equivalent to C_p = 10 μM, 20 μM or 50 μM). NCP solution (1 mL) in a cuvette was titrated by step-wise addition of high concentration stock solution containing chloride salts of the cations, Mg^{2+}, Ca^{2+}, Spd^{3+}, $CoHex^{3+}$ and Spm^{4+} until the maximal level of NCP aggregation was achieved as detected from the static light scattering (SLS) signal intensity increase. The effectiveness of a cation in inducing condensation was quantified by the molar concentration of the ligand needed for a 50% increase in the static light scattering intensity (EC_{50}), see Fig. 2b. Values of EC_{50} were calculated from the titration curves displaying the scattering intensity versus ligand concentration using a sigmoidal fitting. The signal intensity on the Y-axis of the curves were either plotted to scale (Fig. 3c and d) or normalized to 100 (Fig. 2b, Fig. S1,C and Fig. S2). The particle sizes (effective diameters assuming a lognormal distribution) were calculated applying standard theory using the software provided by equipment manufacturer. At least three independent experiments were performed for each cation. Representative graphs are shown in the figures and average values of EC_{50} are reported in the tables.

Precipitation assay (PA)

Precipitation of the NCPs induced by addition of oligocations was studied by an UV absorption monitored assay using a NanoDrop ND-1000 UV/Vis spectrophotometer

(NanoDrop Technologies Inc, Wilmington, DE). A series of solutions (typically 20-24 aliquots of 20 µL each) were prepared containing fixed concentration of the NCP (0.22 mg/mL or 0.552 µM NCP or C_p=162 µM; absorbance at 260 nm A^{260} = 1) and increasing concentration of the chloride salts of the cations (Mg^{2+}, Ca^{2+}, Spd^{3+}, $CoHex^{3+}$ and Spm^{4+}). After 20 min incubation at room temperature, NCP aggregates were precipitated by centrifugation (20,000 g × 10 min). Values of A^{260} were measured from the supernatant. The optical density of the supernatant of the two control solutions of NCP (with and without spinning) in the absence of cation were set as standard, representing null precipitation. Absorbance of the control solutions was equal within experimental uncertainty of the measurements (2-3% according to the NanoDrop specifications). The fraction of NCP remaining in the solution at various cation concentrations was derived by dividing the A_{260} absorbance of each aliquots by that of the standard. At least three independent measurements were carried out for each cation and using two different background buffer solutions: either 10 mM Tris ⊣HCl buffer, pH 7.5 or 10 mM Tris Tris ⊣HCl buffer, pH 7.5 + 10 mM KCl. Results of the precipitation assay were plotted as fraction of NCP remaining in the solution versus concentration of added ligand and fitted by sigmoidal function similar to the light scattering data (Fig. 2a). In some cases full (100%) precipitation is not achieved, and we report the maximum (Max) percentage precipitated as well as $C_{50\%}$ values, which denote the concentration needed to precipitate 50% of the NCP in solution (if the maximum is less than 50%, this is indicated). Representative graphs are shown in the figures and average values of $C_{50\%}$ are reported in the tables. In the case of g-NCP precipitated with divalent cations (maximum precipitation about 40-50%), we verified that the precipitated supernatant could be dialyzed to low salt again, followed by a new PA measurement, with the result that, within experimental accuracy, is the same as the original PA. In all cases, including the g-NCP systems, precipitation is also followed by full resolubilization at higher cation concentrations.

This observation, is common for DNA[65] and that has also been observed for cell extracted NCPs.[11] However, we have not systematically studied this effect, since it occurs under non-physiological conditions and may not be relevant to nucleosomes *in vivo*. These observations for the g-NCP system, which shows incomplete precipitation, indicate that this behavior is an equilibrium process.

Computer modeling

Langevin molecular dynamics simulations were carried using a coarse grained NCP model, force field and simulation setup are given in our earlier work[46,53] (for a detailed description see the supplementary materials of the cited papers.[46,53]

The nucleosome core particle was approximated as a combination of three types of particles. A central sphere represents the globular part of the histone octamer (HO). 25 particles model the nucleosomal DNA wrapped around the HO and 8 strings of connected beads describe the histone N-terminal tails with each bead representing one charge in the histone tail (this model is illustrated in the Supplementary Material, Fig. S4). Each DNA bead (of effective radius 1.0 nm) represents 6 bp DNA and were fixed on the surface of the central particle (of radius 3.5 nm) forming 1.75 superhelix mimicking DNA wrapping around the HO. The original –12e charge of each DNA bead is reduced to –9.44e (total charge –9.44e×25= –236e charge, which is equal to that of the sum of the charges on 147 bp DNA (–294e) plus the globular part of the histone octamer (+58e). This assumes partial neutralization of the DNA charge by the net positive charge of the HO core (see justification and discussion on charge distribution on the HO core in the supplementary material of our previous work).[46] The histone tails were modeled as 8 strings of connected +1e charges of effective radius 0.25 nm and bond length 0.7 nm.[53,60] The number of charged particles in each tail was 9, 14, 11, and 10 to match the charge of the H2A, H2B, H3 and H4 tails respectively.

The described combination of the bead sizes and positioning closely represents the crystallographic structure of the NCP.[1,2] Two models of tailless NCP were tested: the first one was completely tail-free; the second one retained tails. Adoption of these two approaches was used to match the experimental conditions since the respective tails were not completely truncated (see above). Histone acetylations or K→Q mutations at the four lysines of the H4 tail (K5, K8, K12, and K16) were modeled by switching the charges at the positions 5-8 on the corresponding tails. MD simulations were carried out for a cubic simulation cell with a size of 40 nm containing 10 NCPs (the model with starting configuration of ten NCPs is illustrated in Fig. S4 of the Supplementary Material).

Detailed description of the bond potentials as well as the long range (Coulombic) and short range (Lennard-Jones) force parameters is given in our earlier work.[46,53] Simulations were carried out for a cubic simulation cell with a size of 40 nm containing 10 NCPs. The number of ions in the simulation cell with 10 NCP is listed in the Supplementary Material, Tables S1-S3. The concentration of NCPs in the simulation box was 260 μM, which corresponds to about 77 mM in DNA phosphate groups. The systems were simulated for 1.6×10^7 – 3.2×10^7 MD time steps. Configurations for analysis were collected after each 200 steps. Averages were calculated for the final 1.6×10^7 time steps or longer, after achieving convergence in the NCP-NCP radial distribution functions (RDF) and External Tail-Core RDF. To quantify NCP-NCP contacts core-core contact number was used which was calculated by integrating the core-core RDF using threshold 15 nm.[53] Core-core contact number gives estimation of average number of the NCP making close contacts in the simulation cell.

Supplemental material related to this article may be found at …

Acknowledgements

The authors are thankful to Dr. Curt Davey and Prof. Timothy Richmond for gifts of the plasmids encoding DNA and core histones. We are grateful to Dr. Curt Davey and members of his laboratory as well as members of the L.N. laboratory for valuable assistance in production and purification of the DNA, histones and NCPs. Miss Chen Dan is acknowledged for measurements on the NCP-145 construct. We appreciate the Nanyang Technological University High Performance Computer (HPC) Centre for generous allocation of supercomputer time. Discussions with Alexander Lyubartsev are greatly acknowledged. This research was supported by the Singapore Ministry of Education (MOE) through a Tier 2 grant and by the Agency for Science Technology and Research (A*STAR) through BMRC (Biomedical Research Council) grants.

References

1. Luger, K., Mader, A. W., Richmond, R. K., Sargent, D. F. & Richmond, T. J. (1997). Crystal structure of the nucleosome core particle at 2.8 Å resolution. *Nature* **389**, 251-260.
2. Davey, C. A., Sargent, D. F., Luger, K., Maeder, A. W. & Richmond, T. J. (2002). Solvent mediated interactions in the structure of nucleosome core particle at 1.9 Å resolution. *J.Mol.Biol.* **319**, 1097-1113.
3. Vasudevan, D., Chua, E. Y. & Davey, C. A. (2010). Crystal structures of nucleosome core particles containing the '601' strong positioning sequence. *J.Mol.Biol.* **403**, 1-10.
4. Luger, K. & Richmond, T. J. (1998). The histone tails of the nucleosome. *Curr.Opin.Genet.Dev.* **8**, 140-146.
5. Woodcock, C. L. & Dimitrov, S. (2001). Higher-order structure of chromatin and chromosomes. *Curr.Opin.Genet.Dev.* **11**, 130-135.
6. Hansen, J. C. (2002). Conformational dynamics of the chromatin fiber in solution: determinants, mechanisms, and functions. *Annu.Rev.Biophys.Biomol.Struct.* **31**, 361-392.
7. Wolffe, A. P. & Hayes, J. J. (1999). Chromatin disruption and modification. *Nucleic Acids Res.* **27**, 711-720.

8. Horn, P. J. & Peterson, C. L. (2002). Chromatin higher order folding: Wrapping up transcription. *Science* **297**, 1824-1827.
9. Wolffe, A. P. (1998). *Chromatin: Structure and function*. 3rd edit, Academic Press, San Diego, CA.
10. Raspaud, E., Chaperon, I., Leforestier, A. & Livolant, F. (1999). Spermine-induced aggregation of DNA, nucleosome, and chromatin. *Biophys.J.* **77**, 1547-1555.
11. de Frutos, M., Raspaud, E., Leforestier, A. & Livolant, F. (2001). Aggregation of nucleosomes by divalent cations. *Biophys.J.* **81**, 1127-1132.
12. Mangenot, S., Leforestier, A., Vachette, P., Durand, D. & Livolant, F. (2002). Salt-induced conformation and interaction changes of nucleosome core particles. *Biophys.J.* **82**, 345-356.
13. Mangenot, S., Raspaud, E., Tribet, C., Belloni, L. & Livolant, F. (2002). Interactions between isolated nucleosome core particles. A tail bridging effect? *Eur.Phys.J.E* **7**, 221-231.
14. Mangenot, S., Leforestier, A., Durand, D. & Livolant, F. (2003). X-ray diffraction characterization of the dense phases formed by nucleosome core particles. *Biophys.J.* **84**, 2570-2584.
15. Mangenot, S., Leforestier, A., Durand, D. & Livolant, F. (2003). Phase diagram of nucleosome core particles. *J.Mol.Biol.* **333**, 907-916.
16. Bertin, A., Leforestier, A., Durand, D. & Livolant, F. (2004). Role of histone tails in the conformation and interaction of nucleosome core particles. *Biochemistry* **43**, 4773-4780.
17. Bertin, A., Renouard, M., Pedersen, J. S., Livolant, F. & Durand, D. (2007). H3 and H4 histone tails play a central role in the interactions of recombinant NCPs. *Biophys.J.* **92**, 2633-2645.
18. Bertin, A., Mangenot, S., Renouard, M., Durand, D. & Livolant, F. (2007). Structure and phase diagram of nucleosome core particles aggregated by multivalent cations. *Biophys.J.* **93**, 3652-3663.
19. Bertin, A., Durand, D., Renouard, M., Livolant, F. & Mangenot, S. (2007). H2A and H2B tails are essential to properly reconstitute nucleosome core particles. *Eur.Biophys.J.* **36**, 1083-1094.
20. Finch, J. T., Brown, R. S., Richmond, T. J., Rushton, B., Lutter, L. C. & Klug, A. (1981). X-ray diffraction study of a new crystal form of the nucleosome core showing higher resolution. *J.Mol.Biol.* **145**, 757-769.

21. Finch, J. T., Lutter, L. C., Rhodes, D., Brown, R. S., Rushton, B., Levitt, M. & Klug, A. (1977). Structure of nucleosome core particles of chromatin. *Nature* **269**, 29-36.
22. Schalch, T., Duda, S., Sargent, D. F. & Richmond, T. J. (2005). X-ray structure of a tetranucleosome and its implications for the chromatin fibre. *Nature* **436**, 138-141.
23. Robinson, P. J. J., Fairall, L., Huynh, V. A. T. & Rhodes, D. (2006). EM measurements define the dimensions of the "30-nm" chromatin fiber: Evidence for a compact, interdigitated structure. *Proc.Natl.Acad.Sci.U.S.A.* **103**, 6506-6511.
24. Dorigo, B., Schalch, T., Kulangara, A., Duda, S., Schroeder, R. R. & Richmond, T. J. (2004). Nucleosome arrays reveal the two-start organization of the chromatin fiber. *Science* **306**, 1571-1573.
25. Pelta, J., Durand, D., Doucet, J. & Livolant, F. (1996). DNA mesophases induced by spermidine: structural properties and biological implications. *Biophys.J.* **71**, 48-63.
26. Leforestier, A. & Livolant, F. (1997). Liquid crystalline ordering of nucleosome core particles under macromolecular crowding conditions: evidence for a discotic columnar hexagonal phase. *Biophys. J.* **73**, 1771–1776.
27. Leforestier, A., Dubochet, J. & Livolant, F. (2001). Bilayers of nucleosome core particles. *Biophys.J.* **81**, 2114-2421.
28. Raspaud, E., Pitard, B., Durand, D., Aquerre-Chariol, O., Pelta, J., Byk, G., Scherman, D. & Livolant, F. (2001). Polymorphism of DNA/multi-cationic lipid complexes driven by temperature and salt. *J.Phys.Chem.B* **105**, 5291-5297.
29. Turner, B. M. (1991). Histone acetylation and control of gene expression. *J.Cell Sci.* **99**, 13-20.
30. Kurdistani, S. K., Tavazole, S. & Grunstein, M. (2004). Mapping global histone acetylation patterns to gene expression. *Cell* **117**, 721-733.
31. Calestagne-Morelli, A. & Ausio, J. (2006). Long-range histone acetylation: biological significance, structural implications, and mechanisms. *Biochem.Cell Biol.* **84**, 518-527.
32. Szerlong, H. J., Prenni, J. E., Nyborg, J. K. & Hansen, J. C. (2010). Activator-dependent p300 acetylation of chromatin in vitro: enhancement of transcription by disruption of repressive nucleosome-nucleosome interactions. *J.Biol.Chem.* **285**, 31954-31964.
33. Lewis, P. N., Guillementte, J. G. & Chan, S. (1988). Histone accessibility determined by lysine-specific acetylation in chicken erythrocyte nuclei. *Eur.J.Biochem.* **172**, 135-145.

34. Perry, M. & Chalkley, R. (1981). The effect of histone hyperacetylation on the nuclease sensitivity and the solubility of chromatin. *J.Biol.Chem.* **256**, 3313-3318.
35. Perry, M. & Chalkley, R. (1982). Histone acetylation increases the solubility of chromatin and occurs sequentially over most of the chromatin. A novel model for the biological role of histone acetylation. *J.Biol.Chem.* **257**, 7336-7347.
36. Tse, C., Sera, T., Wolffe, A. P. & Hansen, J. C. (1998). Disruption of higher-order folding by core histone acetylation dramatically enhances transcription of nucleosomal arrays by RNA polymerase III. *Mol.Cell.Biol.* **18**, 4629-4638.
37. Wang, X., He, C., Moore, S. C. & Ausio, J. (2001). Effects of histone acetylation on the solubility and folding of the chromatin fiber. *J.Biol.Chem.* **276**, 12764-1268.
38. Pesavento, J. J., Bullock, C. R., LeDuc, R. D., Mizzen, C. A. & Kelleher, N. L. (2008). Combinatorial modification of human histone H4 quantitated by two-dimensional liquid chromatography coupled with top down mass spectrometry. *J.Biol.Chem.* **283**, 14927-14937.
39. Jiang, L., Smith, J. N., Anderson, S. L., Ma, P., Mizzen, C. A. & Kelleher, N. L. (2007). Global assessment of combinatorial post-translational modification of core histones in yeast using contemporary mass spectrometry. LYS4 trimethylation correlates with degree of acetylation on the same H3 tail. *J.Biol.Chem.* **282**, 27923-27934.
40. Shogren-Knaak, M. A., Ishii, H., Sun, J.-M., Pazin, M., Davie, J. R. & Peterson, C. L. (2006). Histone H4-K16 acetylation controls chromatin structure and protein interactions. *Science* **311**, 844-847.
41. Kan, P.-Y., Lu, X., Hansen, J. C. & Hayes, J. J. (2007). The H3 tail domain participates in multiple interactions during folding and self-association of nucleosome arrays. *Mol.Cell.Biol.* **27**, 2084–2091.
42. Wang, X. & Hayes, J. J. (2007). Site-specific binding affinities within the H2B tail domain indicate specific effects of lysine acetylation. *J.Biol.Chem.* **282**, 32867–32876.
43. Routh, A., Sandin, S. & Rhodes, D. (2008). Nucleosome repeat length and linker histone stoichiometry determine chromatin fiber structure. *Proc.Natl.Acad.Sci.U.S.A.* **105**, 8872-8877.
44. Robinson, P. J. J., An, W., Routh, A., Martino, F., Chapman, L., Roeder, R. G. & Rhodes, D. (2008). 30 nm chromatin fibre decompaction requires both H4-K16 acetylation and linker histone eviction. *J.Mol.Biol.* **381**, 816-825.

45. Wang, X. & Hayes, J. J. (2008). Acetylation mimics within individual core histone tail domains indicate distinct roles in regulating stability of higher-order chromatin structure. *Mol.Cell.Biol.* **28**, 227-236.

46. Korolev, N., Allahverdi, A., Yang, Y., Fan, Y., Lyubartsev, A. P. & Nordenskiöld, L. (2010). Electrostatic origin of salt-induced nucleosome array compaction. *Biophys. J.* **99** 1896-1905.

47. Allahverdi, A., Yang, R., Korolev, N., Fan, Y., Davey, C. A., Liu, C. F. & Nordenskiöld, L. (2011). The effects of histone H4 tail acetylations on cation-induced chromatin folding and self-association. *Nucleic Acids Res.* **39**, 1680–1691

48. Shimko, J. C., North, J. A., Bruns, A. N., Poirier, M. G. & Ottesen, J. J. (2011). Preparation of fully synthetic histone H3 reveals that acetyl-lysine 56 facilitates protein binding within nucleosomes. *J.Mol.Biol.* **408**, 187-204.

49. Pollard, K. J., Samuels, M. L., Crowley, K. A., Hansen, J. C. & Peterson, C. L. (1999). Functional interaction between GCN5 and polyamines: a new role for core histone acetylation. *EMBO J.* **18**, 5622-5633.

50. Dorigo, B., Schalch, T., Bystricky, K. & Richmond, T. J. (2003). Chromatin fiber folding: requirement for the histone H4 N-terminal tail. *J.Mol.Biol.* **327**, 85-96.

51. McBryant, S. J., Klonoski, J., Sorensen, T. C., Norskog , S. S., Williams, S., Resch, M. G., Toombs, J. A., 3rd, Hobdey , S. E. & Hansen, J. C. (2009). Determinants of histone H4 N-terminal domain function during nucleosomal array oligomerization: roles of amino acid sequence, domain length, and charge density. *J.Biol.Chem.* **284**, 16716-16722.

52. Lowary, P. T. & Widom, J. (1998). New DNA sequence rules for high affinity binding to histone octamer and sequence-directed nucleosome positioning. *J.Mol.Biol.* **276**, 19-42.

53. Yang, Y., Lyubartsev, A. P., Korolev, N. & Nordenskiöld, L. (2009). Computer modeling reveals that modifications of the histone tail charges define salt-dependent interaction of the nucleosome core particles. *Biophys.J.* **96**, 2082-2094.

54. Sen, D. & Crothers, D. M. (1986). Condensation of chromatin: Role of multivalent cations. *Biochemistry* **25**, 1495-1503.

55. Korolev, N., Berezhnoy, N. V., Eom, K. D., Tam, J. P. & Nordenskiöld, L. (2009). A universal description for the experimental behavior of salt-(in)dependent oligocation-induced DNA condensation. *Nucleic Acids Res.* **37**, 7137–7150.

56. Korolev, N., Lyubartsev, A. P. & Nordenskiöld, L. (2010). Cation-induced polyelectrolyte-polyelectrolyte attraction in solutions of DNA and nucleosome core particles. *Adv.Colloid Interface Sci.* **158**, 32–47.
57. Bloomfield, V. A. (1997). DNA condensation by multivalent cations. *Biopolymers* **44**, 269-282.
58. Rau, D. C. & Parsegian, V. A. (1992). Direct measurement of the intermolecular forces between counterion-condensed DNA double helices. Evidence for long-range attractive forces. *Biophys.J.* **61**, 246-259.
59. Yang, C., van der Woerd, M. J., Muthurajan, U. M., Hansen, J. C. & Luger, K. (2011). Biophysical analysis and small-angle X-ray scattering-derived structures of MeCP2-nucleosome complexes. *Nucleic Acids Res.* **in press**, doi:10.1093/nar/gkr005.
60. Korolev, N., Lyubartsev, A. P. & Nordenskiöld, L. (2006). Computer modeling demonstrates that electrostatic attraction of nucleosomal DNA is mediated by histone tails. *Biophys.J.* **90**, 4305-4316.
61. Luger, K., Rechsteiner, T. J. & Richmond, T. J. (1999). Preparation of nucleosome core particle from recombinant histones. *Methods Enzymol.* **304**, 3-19.
62. Luger, K., Rechsteiner, T. & Richmond, T. J. (1999). Expression and purification of recombinant histones and nucleosome reconstitution. *Methods Mol.Biol.* **119**, 1-16.
63. Dyer, P. N., Edayathumangalam, R. S., White, C. L., Bao, Y., Chakravarthy, S., Muthurajan, U. M. & Luger, K. (2004). Reconstitution of nucleosome core particles from recombinant histones and DNA. *Methods Enzymol.* **375**, 23-44.
64. Huang, D., Korolev, N., Eom, K. D., Tam, J. P. & Nordenskiöld, L. (2008). Design and biophysical characterization of novel polycationic ε-peptides for DNA compaction and delivery. *Biomacromolecules* **9**, 321-330.
65. Raspaud, E., Olvera de la Cruz, M., Sikorav, J.-L. & Livolant, F. (1998). Precipitation of DNA by polyamines: a polyelectrolyte behavior. *Biophys.J.* **74**, 381-393.

Figure Legends

Fig. 1. NCP-NCP stacking observed in the NCP crystals. The 1AOI[1] coordinates was used as an example. In all published NCP crystals, the histone tails are not fully resolved. However, most NCP crystals report a structure where the K16-R23 domain of the H4 histone in the NCP1 is located between the surfaces of the two nucleosomes and interacting with the H2A acidic patch of the NCP2. This H4 K16-R23 domain (magenta, with crucial NZ atom of the H4-K16 as blue sphere) and oxygen atoms (small red spheres) of carboxylate groups forming electronegative patch is shown as insert in (**a**) and its location is marked by ovals in (**a-c**). Cartoons (**a**), (**b**) and (**c**) show different projections of the NCP1 – NCP2 contact.

Fig. 2. Aggregation of the wt-NCP caused by addition of oligocations monitored by (**a**) precipitation assay (related EC_{50} data, see Table 1, row 5) and (**b**) light scattering (EC_{50} data, Table 1, row 3). Cations (Mg^{2+}, Ca^{2+}, Spd^{3+}, $CoHex^{3+}$ and Spm^{4+}) are indicated in the graphs; points are experimental values, curves are sigmoidal fitting of the data; titrations were carried in buffer containing 10 mM KCl, 10 mM Tris·HCl, pH 7.5; (**a**) NCP concentration (C_{NCP}) is 0.11 mg/mL (C_p=162 μM); (**b**) C_{NCP} = 6.8 μg/mL (C_p=10 μM). The human 147 bp α-satellite DNA was used to prepare NCPs.

Fig. 3. Comparison of the wt-NCP (stars) and g-NCP (circles) aggregation monitored by PA for Ca^{2+} (**a**) and $CoHex^{3+}$ (**b**) ($C_{50\%}$ data, Table 2) and light scattering for Mg^{2+} and Ca^{2+} (**c**) and $CoHex^{3+}$ (**d**) (EC_{50} data, Table 3). NCP type and cation are indicated for each curve in the graphs. The NCP solution contained either 10 mM Tris·HCl, pH 7.5 (Tris) or 10 mM Tris·HCl, pH 7.5 + 10 mM KCl (Tris + K^+) as indicated for each titration curve. NCPs reconstituted with the human 147 bp α-satellite DNA was used. The NCP concentration was respectively 162 μM and 50 μM (in DNA phosphate) for the PA and SLS titrations.

Fig. 4. Comparison of the aggregation behavior of NCPs with different modifications in the H4 histone tail caused by **(a)** addition of Mg^{2+} and **(b)** $CoHex^{3+}$ ($C_{50\%}$ data, Table 2) in 10 mM Tris ·HCl buffer pH 7.5.

Fig. 5. Coarse-grained molecular dynamics simulation of the nucleosome core particle solutions in the presence of various cations. (**a**) Representative snapshots showing typical distributions of the NCPs in the simulation cell at given concentration of cations (indicated near snapshots). The first row displays the results for the systems of the globular NCP (g-NCP); second row is the data for the NCP with fully charged tails (wt-NCP). (**b**). Comparison of the core-core RDFs of the wt-NCP (solid curves) and g-NCP (dashed lines) in the presence of Mg^{2+} (blue curves) or $CoHex^{3+}$ (red). The concentrations of Mg^{2+} and $CoHex^{3+}$ in the simulation cell are as indicated in the corresponding snapshots in (**a**). Sketches near the RDF peaks illustrate the types of the respective NCP-NCP contacts. (**c**). External tail-core RDFs for the simulated systems of wt-NCPs with various cations. For each sort of cation, the respective RDF was calculated at cation concentration indicated near the corresponding snapshot of the wt-NCP in panel (**a**).

Fig. 6. Dependencies on concentration of Mg^{2+} (blue) or $CoHex^{3+}$ (red) of (**a**) core-core contact number and (**b**) magnitudes of maximum in external tail-core RDFs for titrations of systems with 10 wt-NCPs (stars) or g-NCPs (hollow squares).

Fig. 7. Purity check of (**a**) refolding of the wild type and globular histone octamer and (**b**) NCP reconstitution using the human 147 bp α-satellite DNA. (**a**). Histone octamers (wt-HO and g-HO) were checked on 18% SDS PAGE. Lane 1 shows three bands corresponding to (from top to bottom) H3, H2A/H2B and H4. Lane 2 shows globular histones. Globular histones run faster

than the wild-type histones due to tail truncation. (**b**). Native PAGE (5%) of reconstituted wt NCP and g-NCP.

List of Tables

Table 1. EC_{50} values obtained by the static light scattering (SLS) and precipitation assay (PA) titrations for the wt-NCP reconstituted with 147 and 145 bp DNA in 10 mM Tris ⋅HCl (pH 7.5) solution in the absence (Tris) and in the presence of 10 mM KCl (Tris + KCl).

Table 2. Summary of precipitation assay results using NCP reconstituted with different variants of the H4 histone and 147 bp α-satellite DNA.

Table 3 Summary of the light scattering titration results using NCP reconstituted with different variants of the H4 histone and 147 bp α-satellite DNA.

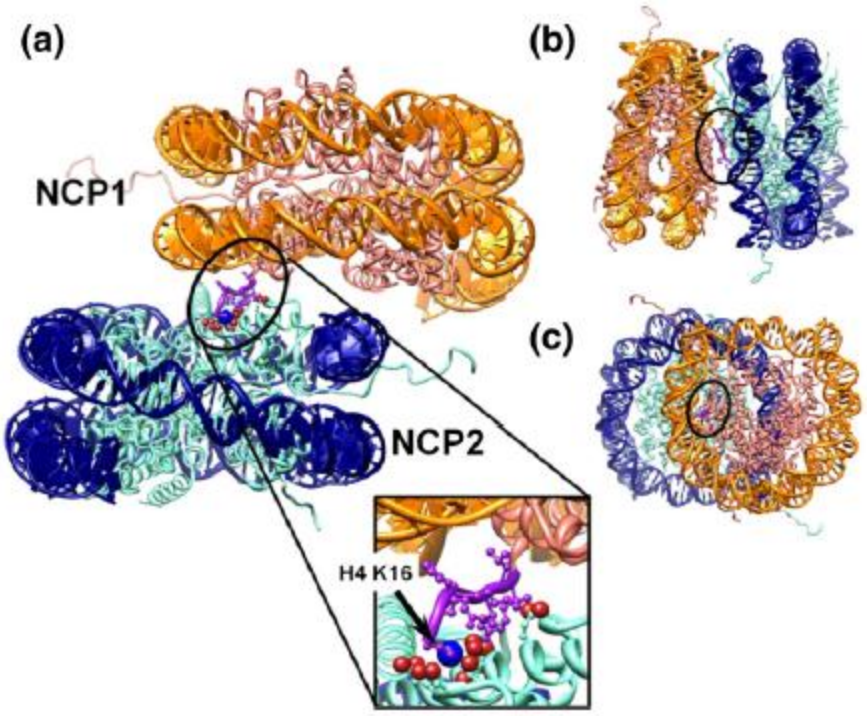

Fig. 1

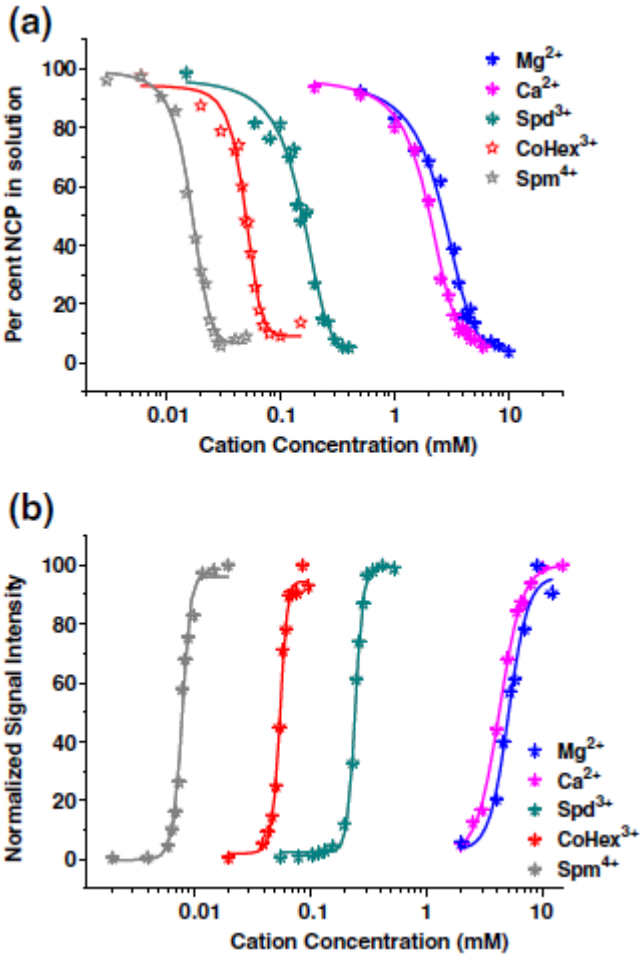
(a)
Per cent NCP in solution
100
80
60
40
20
0
0.01
0.1
1
10
Cation Concentration (mM)
Mg2+
Ca2+
Spd3+
CoHex3+
Spm4+
(b)
Normalized Signal Intensity
100
80
60
40
20
0
0.01
0.1
1
10
Cation Concentration (mM)
Mg2+
Ca2+
Spd3+
CoHex3+
Spm4+

Fig. 2

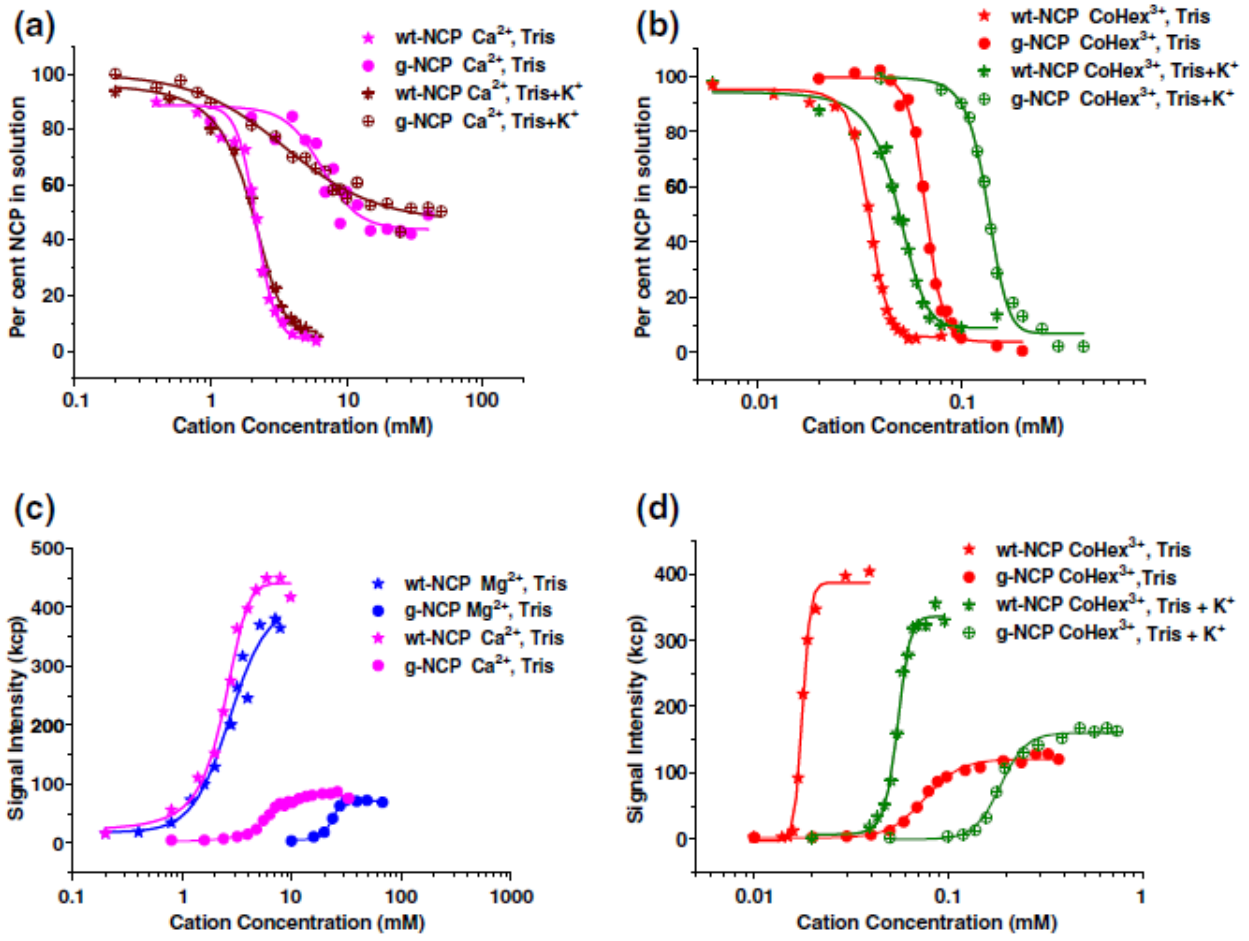
(a)
wt-NCP Ca2+, Tris
g-NCP Ca2+, Tris
wt-NCP Ca2+, Tris+K+
g-NCP Ca2+, Tris+K+
Per cent NCP in solution
Cation Concentration (mM)
(b)
wt-NCP CoHex3+, Tris
g-NCP CoHex3+, Tris
wt-NCP CoHex3+, Tris+K+
g-NCP CoHex3+, Tris+K+
Per cent NCP in solution
Cation Concentration (mM)
(c)
wt-NCP Mg2+, Tris
g-NCP Mg2+, Tris
wt-NCP Ca2+, Tris
g-NCP Ca2+, Tris
Signal Intensity (kcp)
Cation Concentration (mM)
(d)
wt-NCP CoHex3+, Tris
g-NCP CoHex3+,Tris
wt-NCP CoHex3+, Tris + K+
g-NCP CoHex3+, Tris + K+
Signal Intensity (kcp)
Cation Concentration (mM)

Fig. 3

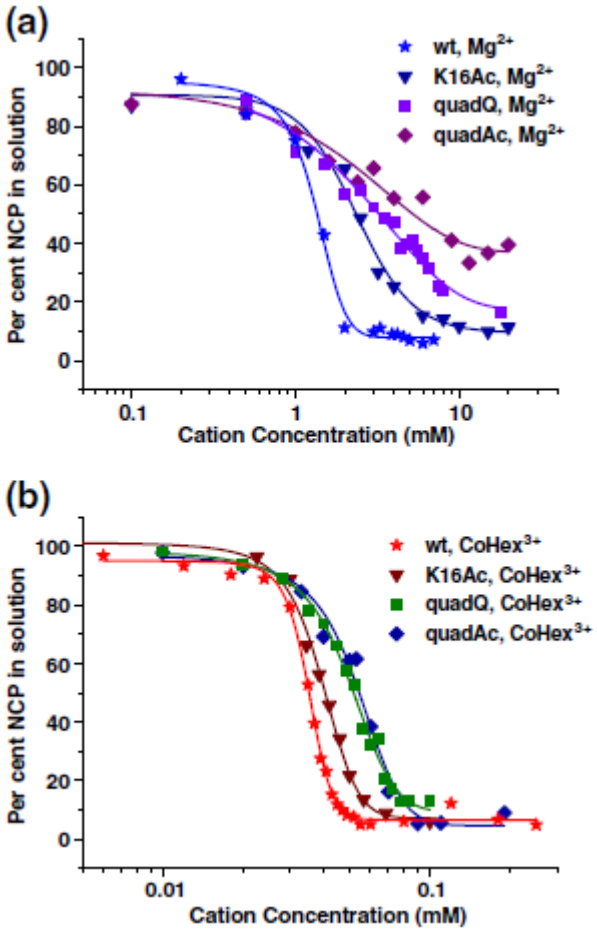
(a)
wt, Mg2+
K16Ac, Mg2+
quadQ, Mg2+
quadAc, Mg2+
Per cent NCP in solution
100
80
60
40
20
0
0.1
1
10
Cation Concentration (mM)
(b)
wt, CoHex3+
K16Ac, CoHex3+
quadQ, CoHex3+
quadAc, CoHex3+
Per cent NCP in solution
100
80
60
40
20
0
0.01
0.1
Cation Concentration (mM)

Fig. 4

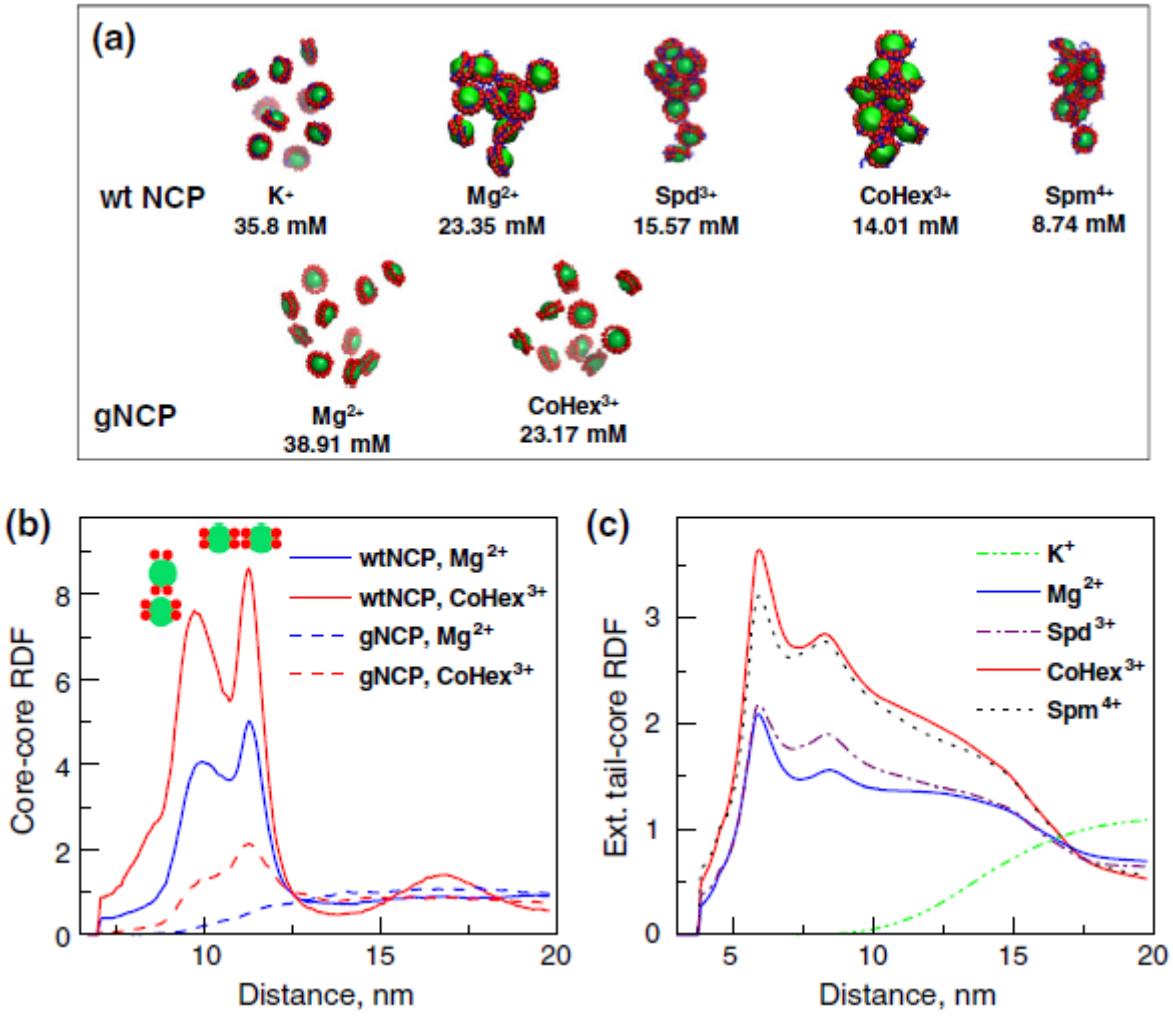
(a)
wt NCP
K+
35.8 mM
Mg2+
23.35 mM
Spd3+
15.57 mM
CoHex3+
14.01 mM
Spm4+
8.74 mM
gNCP
Mg2+
38.91 mM
CoHex3+
23.17 mM
(b)
wtNCP, Mg2+
wtNCP, CoHex3+
gNCP, Mg2+
gNCP, CoHex3+
Core-core RDF
Distance, nm
(c)
K+
Mg2+
Spd3+
CoHex3+
Spm4+
Ext. tail-core RDF
Distance, nm

Fig. 5

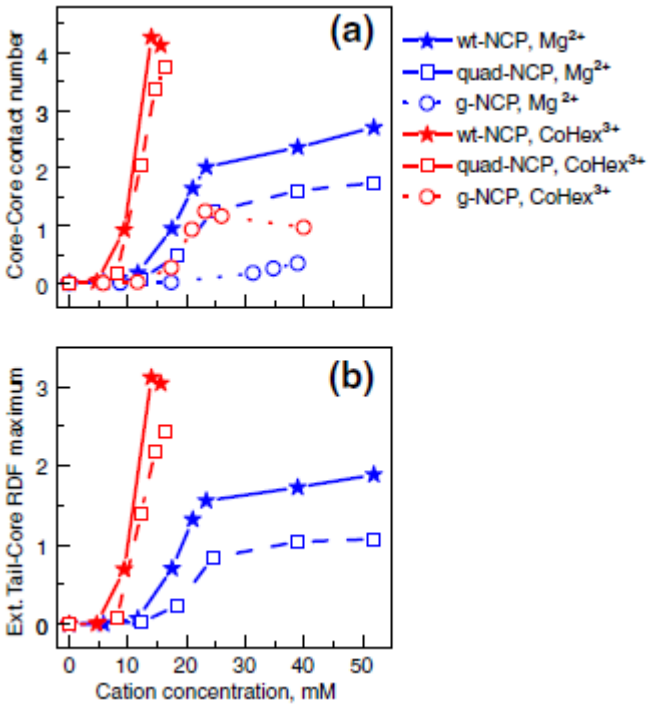
(a)
Core-Core contact number
0
1
2
3
4
wt-NCP, Mg2+
quad-NCP, Mg2+
g-NCP, Mg 2+
wt-NCP, CoHex3+
quad-NCP, CoHex3+
g-NCP, CoHex3+
(b)
Ext. Tail-Core RDF maximum
0
1
2
3
0
10
20
30
40
50
Cation concentration, mM

Fig. 6

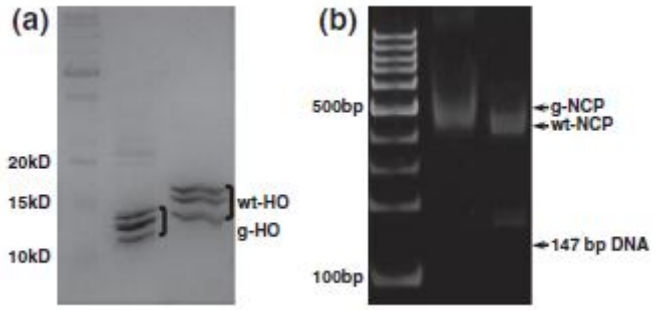

Fig. 7

Conditions		Cations									
		Mg^{2+} (mM)		Ca^{2+} (mM)		Spd^{3+} (μM)		$CoHex^{3+}$ (μM)		Spm^{4+} (μM)	
		147 bp	145 bp	147 bp	145 bp	147 bp	145 bp	147 bp	145 bp	147 bp	145 bp
SLS	Tris; C_P = 20 μM	4.2 ± 0.4	2.3 ± 0.2	3.1 ± 0.1	2.6 ± 0.4	108 ± 10	78 ± 4	20.7 ± 2.3	22.3 ± 3.3	3.9 ± 0.3	3.8 ± 0.2
	Tris; C_P = 10 μM	4.3 ± 0.3	—	3.4 ± 0.03	—	68 ± 6	—	18.8 ± 2.3	—	2.5 ± 0.1	—
	Tris + KCl; C_P = 10 μM	4.9 ± 0.2	—	4.3 ± 0.2	—	236 ± 6	—	54.4 ± 1.0	—	7.7 ± 0.3	—
PA[a]	Tris; C_P = 162 μM	1.4 ± 0.2	1.7 ± 0.3	2.0 ± 0.1	1.6 ± 0.3	112 ± 2	78 ± 6	37.2 ± 1.9	33.0 ± 0.8	16.9 ± 1.6	15.8 ± 0.2
	Tris + KCl; C_P = 162 μM	2.5 ± 0.1	—	2.1 ± 0.1	—	164 ± 24	—	59.5 ± 15.9	—	17.7 ± 2.1	—

Values represent the average of at least three independent measurements.
[a] For Mg^{2+} and Ca^{2+} where incomplete precipitation was observed, EC_{50} values corresponding to the cation concentration at 50% precipitation are given.

Table 1

Conditions		Cations					
		Mg^{2+}		Ca^{2+}		$CoHex^{3+}$	
		$C_{50\%}$ (mM)	Max (%)	$C_{50\%}$ (mM)	Max (%)	$C_{50\%}$ (μM)	Max (%)
Tris	wt-NCP	1.4 ± 0.2	98	2.0 ± 0.01	97	37.2 ± 1.9	97
	K16Ac-NCP	2.3 ± 0.1	95	—	—	43.3 ± 3.0	94
	quadQ-NCP	3.1 ± .02	84	2.9 ± 0.5	92	52.8 ± 1.2	97
	quadAc-NCP	5.9 ± 0.6	74	—	—	55.1 ± 0.8	94
	g-NCP	20.9 ± 4.4	50.5	13.0 ± 1.3	60	66.6 ± 1.9	100
	147-bp DNA	44.7 ($C_{23.6\%}$)[a]	23.6	81.5 ($C_{23\%}$)[a]	23	94.1 ± 0.7	99
Tris + KCl	wt-NCP	2.5 ± 0.1	96	2.1 ± 0.1	95	59.5 ± 15.9	91
	g-NCP	25.0 ($C_{39.5\%}$)[a]	39.5	24.0 ± 6.9	55	127 ± 5.9	99

The experiment was conducted at two different buffer conditions as in Table 1. Cation concentrations at 50% NCP precipitation ($C_{50\%}$) from at least three independent measurements are shown, with maximal degree of NCP precipitation (Max) is also indicated

[a] $C_{50\%}$ cannot be obtained, since maximal precipitation is below 50%. Values given are the cation concentration at maximal precipitation (C_{Max}).

Table 2

Sample	Mg^{2+}			Ca^{2+}			$CoHex^{3+}$		
	C_P (μM)	EC_{50} (mM)	I_{max} (kcp)	C_P (μM)	EC_{50} (mM)	I_{max} (kcp)	C_P (μM)	EC_{50} (μM)	I_{max} (kcp)
wt-NCP	20	4.2±0.4	337	20	3.1±0.1	293	10	18.8±2.3	705
	50	2.3±0.4	380	50	2.3±0.3	480	20	20.7±2.3	719
quadQ-NCP	20	1.1±0.1	183	20	1.0±0.04	182	20	32.9±1.0	540
g-NCP	50	21.1±2.9	148	50	7.4±3.0	123	10	70.2±6.4	120

The experiment was conducted in 10 mM Tris–HCl (pH 7.5) with typical (C_P = 20 μM) and high (C_P = 50 μM) NCP concentrations; I_{max} is the maximal intensity of the scattering signal observed in SLS titration curve. Values represent the average of at least three independent measurements.

Table 3